The munc13-4–rab27 complex is specifically required for tethering secretory lysosomes at the plasma membrane

Edo D. Elstak,[1] *Maaike Neeft,[1] *Nadine T. Nehme,[2] Jarno Voortman,[3] Marc Cheung,[1] Monireh Goodarzifard,[1] Hans C. Gerritsen,[4] Paul M. P. van Bergen en Henegouwen,[3] Isabelle Callebaut,[5] Geneviève de Saint Basile,[2,6] and Peter van der Sluijs[1]

[1]Department of Cell Biology, University Medical Center Utrecht, Utrecht, The Netherlands; [2]Inserm and Université Paris Descartes, Faculté de Médecine, Paris, France; [3]Department of Biology, Science Faculty, University of Utrecht, Utrecht, The Netherlands; [4]Department of Molecular Biophysics, University of Utrecht, Utrecht, The Netherlands; [5]Université Pierre et Marie Curie, Centre National de la Recherche Scientifique, Paris, France; and [6]Centre d'Etude des Déficits Immunitaires, Assistance Publique des Hôpitaux de Paris, Hôpital Necker-Enfants Malades, Paris, France

Cytotoxic T lymphocytes (CTLs) kill target cells through the polarized release of lytic molecules from secretory lysosomes. Loss of munc13-4 function inhibits this process and causes familial hemophagocytic lymphohistiocytosis type 3 (FHL3). munc13-4 binds rab27a, but the necessity of the complex remains enigmatic, because studies in knockout models suggest separate functions. In the present study, we describe a noncanonical rab27a-binding motif in the N-terminus of munc13-4. Point mutants in this sequence have severely impaired rab27a binding, allowing dissection of rab27a requirements in munc13-4 function. The munc13-4–rab27a complex is not needed for secretory lysosome maturation, as shown by complementation in CTLs from FHL3 patients and in a mast cell line silenced for munc13-4. In contrast, fusion of secretory lysosomes with, and content release at the plasma membrane during degranulation, strictly required the munc13-4–rab27a complex. Total internal reflection fluorescence microscopy imaging revealed that the complex corrals motile secretory lysosomes beneath the plasma membrane during degranulation and controls their docking. The propensity to stall motility of secretory lysosomes is lost in cells expressing munc13-4 point mutants that do not bind rab27. In summary, these results uncovered a mechanism for tethering secretory lysosomes to the plasma membrane that is essential for degranulation in immune cells. (*Blood*. 2011;118(6): 1570-1578)

Introduction

Natural killer (NK) cells and cytotoxic T lymphocytes (CTLs) are critical for immune responses against virus infections and cell transformation.[1] The cytotoxic function is exerted through recognition of target cells, followed by regulated exocytosis of granzymes and perforin that causes apoptosis of the APC. The effector molecules are stored in lytic granules, otherwise known as secretory lysosomes or lysosome-related organelles. Their molecular makeup comprises an acidic, proteoglycan core, soluble lysosomal enzymes, and lysosome-associated membrane proteins.[2] The efficient removal of target cells via the granule-dependent pathway also serves an important function in homeostasis of lymphocytes. Genetic defects affecting cytotoxicity cause persistent release of cytokines, including IFN-γ, IL-6, IL-18, and TNF; uncontrolled expansion of $CD8^+$ T lymphocytes; and life-threatening macrophage activation syndrome.[3]

After binding an APC, secretory lysosomes relocate along microtubules to the microtubule organizing center that polarizes toward the target cell. The centrosome and associated secretory lysosomes translocate together to the contact patch between effector and target cell, where docking of the centrosome delivers secretory lysosomes for fusion.[4,5] This so-called immunologic synapse comprises a large, concentrically organized supramolecular complex in which cell adhesion molecules make up the peripheral zone, whereas signaling proteins localize to the central core, where secretory lysosomes dock and fuse.[6] munc13-4 and rab27a are essential for the regulated release of secretory lysosomes in CTLs and NK cells.[7-9]Genetic deficiency in munc13-4 and rab27a underlie the uncontrolled lymphocyte proliferation and activation observed in familial hemophagocytic lymphohistiocytosis type 3 (FHL3) and Griscelli syndrome type 2 (GS2), respectively.[7,8]

rab27a is thought to be important for directing secretory lysosomes to the immunologic synapse and perhaps for their release from microtubules. In munc13-4–deficient, cytotoxic lymphocytes, secretory lysosomes appear to dock on, but do not fuse with, the plasma membrane.[8] munc13-4 also regulates the assembly of an exocytic precursor organelle from rab11- and rab7/rab27–containing endosomes that is needed for the maturation of secretory lysosomes into a fusion-competent lytic organelle.[10] Rab GTPases are bimolecular switches, the active conformations of which regulate membrane organization, protein sorting, and signaling through the recruitment of often tissue-specific effector proteins.[11] Multiple effectors have been identified for rab27,[12,13] of which 3, including munc13-4, are expressed in cytotoxic lymphocytes.[14,15] Through the timed association with distinct effectors such as munc13-4, slp1, slp2-a, and perhaps a myosin, rab27a can regulate the outcome of multiple cellular processes. Ultimately, the coordinating function of rab27a positions secretory lysosomes at

Submitted February 25, 2011; accepted June 4, 2011. Prepublished online as *Blood* First Edition paper, June 21, 2011; DOI 10.1182/blood-2011-02-339523.

*M.N. and N.T.N. contributed equally to this study.

The online version of this article contains a data supplement.

The publication costs of this article were defrayed in part by page charge payment. Therefore, and solely to indicate this fact, this article is hereby marked "advertisement" in accordance with 18 USC section 1734.

the immunologic synapse and causes their fusion with the plasma membrane.

The molecular principles and signals underlying the directed membrane trafficking during secretory lysosome degranulation are not clear, and are controversial with respect to the functional relationship between rab27s and munc13-4. Knockouts of rab27a/b and munc13-4 produce different secretion phenotypes in platelets,[16,17] whereas in neutrophils, munc13-4 regulates the motility of rab27 granules.[18] In CTLs and NK cells, rab27a and munc13-4 do not localize to lytic granules unless the cells are "activated." Separate signaling routes are used in NK cells to direct munc13-4 and rab27 to lytic granules,[19,20] whereas munc13-4 and rab27a associate independently with membrane.[10,21] In the present study, we identified a noncanonical rab27-binding region in munc13-4 that is required and sufficient for rab27a binding. Critical point mutants in this motif revealed an essential function of the munc13-4–rab27a complex in tethering secretory lysosomes to the plasma membrane and in degranulation.

Methods

Constructs

cDNAs encoding human rab11, rab27a, munc13-4, pMD2.G, and psPAX2 have been described previously.[22,23] Expression constructs and ala mutants of munc13-4 were generated by PCR and subcloned in pcDNA3.1HisB and pEGFP-C2. The following cDNAs were generously provided by the indicated colleagues: pEF-BOS-Flag-rab27a (Mitsunori Fukuda, Fukuda Initiative Research Unit, RIKEN, Japan), Munc13-1 pcDNA3 (Nils Brose, MPI for Experimental Medicine, Göttingen, Germany), and baiap3pcDNA3.1His (Takash Tokino, Institute of Medical Science, Tokyo, Japan). cDNAs encoding fluorescent fusion proteins were extended with Gateway sequences and transferred to the lentiviral plasmid pLNT-SFFV-WPRE-Gateway.[23] All synthetic DNA was verified by dye-termination sequencing of both strands.

Antibodies

The rabbit antibody against green fluorescent protein (GFP) was from BD Biosciences. Mouse mAbs were from the indicated sources: EEA1 and rat CD63 (BD Biosciences), GFP (Roche), and Flag M2 (Sigma-Aldrich), and rat p80 (Juan Bonifacino, National Institutes of Health, Bethesda, MD). Rabbit antibodies against rab27a and munc13-4 have been described previously.[21] Mouse IgE mAbs against DNP (clone SPE-7) were obtained from Sigma-Aldrich. Conjugated secondary antibodies were from Jackson ImmunoResearch Laboratories.

Cells, transfection, and lentiviral transduction

PBMCs were isolated from whole blood sample taken from controls (WT) and from a patient with FHL3 who was described previously (P 83b in Feldmann et al[8]). This patient carries a homozygous one-base deletion (214delC), leading to frameshift and a premature stop codon. Samples were obtained from patients and controls who had provided written informed consent in accordance with procedures at Inserm. CTLs were obtained as described previously,[10] and (co-) transfected using Amaxa nucleofection. Electroporated cell populations were incubated in complete medium for 4 hours and IL-2 was then added. For each individual PBMC population electroporated, the "transfected" cell population designates the cell fraction that coexpresses the vectors whereas the "nontransfected" cell fraction designates cells that do not express the vectors. Efficacy of transfection was ~ 30%. The degranulation assay was performed 6-8 hours after transfection. Lentivirus production in HEK293T cells and transduction of the RBL-2H3 mast cell line were described previously.[23] The following siRNAs (Applied Biosystems) GGAACAAGAUUUUUCACAAtt (siRNA#1), and GUUGAAUGGUUUCACCUGAtt (siRNA#2) were used at 200 pmol to silence munc13-4 in RBL-2H3 cells.[23]

Degranulation assays

To quantify cytotoxic granule exocytosis, CTLs were stimulated with 10 μg/mL of coated anti-CD3 mAbs in the presence of anti-CD107a-FITC and anti–CD107b–FITC mAbs, according to a standard technique.[24] Cells were incubated for 3 hours at 37°C in 5% CO_2. Thereafter, cells were harvested, washed once with PBS and 0.02% azide, stained with anti-CD3–APC and anti-CD8–PE (BD Biosciences), and analyzed by flow cytometry. Cytotoxic granule exocytosis was measured by the induction of CD107 surface expression on CTLs (Δ CD107), calculated as the percentage of $CD107^+$ CTLs stimulated with anti-CD3 and subtracted from the percentage of $CD107^+$ of unstimulated CTLs. Dot plots were gated on $CD3^+CD8^+$ T cells and gates were set individually on the basis of T cells incubated with medium alone. Data were analyzed with FlowJo 8.8.4 software (TreeStar). Degranulation in RBL-2H3 cells was induced with 100nM phorbol 12-myristate 13-acetate (PMA)/1μM ionomycin or 50 ng/mL of IgE and 500 ng/mL of HSA-DNP, and released β-hexosaminidase was measured fluorometrically.[23] Both methods yielded similar β-hexosaminidase secretion efficiencies.

Protein interaction assays

In vitro pull-down experiments were done with GTPγS loaded GST-rab27a produced in *E coli* BL21(DE3) and ^{35}S-labeled proteins generated by in vitro-transcription translation as described previously.[21] Bound proteins were resolved on 10% or 12.5% SDS-PAA gels, visualized by phosphor imaging, and quantitated with ImageQuant software (GE-Healthcare Life Sciences). Normalization was done with respect to the input signal for each mutant. For in vivo binding studies, COS-7 cells were transfected with pEF-BOS-Flag-rab27a with or without peGFP-munc13-4 (aa 240-290) or peGFP-munc13-4 (aa 240-340), After 24 hours, the cells were lysed and immunoprecipitations with Flag-M2 beads (Sigma-Aldrich) and Western blot with GFP antibodies was performed as described previously.[22]

Fluorescence microscopy

Fluorescence microscopy on fixed specimens was performed as described previously.[23] Coverslips were examined with an LSM 510 confocal microscope (Zeiss) using a 63× oil objective or on a Delta vision light microscope equipped with a Xenon lamp and a 100× oil objective, and collected on a chilled emCCD camera (Cascade; Photometrics). Detectors were set to detect an optimal signal below the saturation limits. Image sets to be compared were acquired during the same session and using the same acquisition settings. Images were deconvoluted using Softworx software (3.7.13EL); ratio aggressive, 15 iterations.

TIRF microscopy

For total internal reflection fluorescence (TIRF) experiments, we used an objective-type TIRF system based on an inverted microscope (Eclipse TE2000-U; Nikon) equipped with an oil-immersion objective (plan apo 60×, numerical aperture 1.49; Nikon). Specimens were illuminated with a model 161C-030 argon laser (Spectraphysics) with an excitation power between 10 and 30 μW. Excitation light was separated with a dichroic mirror (Nikon B-2A) from fluorescent light originated from the sample, and photons were collected on the chilled emCCD camera. Winview Version 5.4 software was used to acquire, display, and process the images. Images were recorded (EM gain 3000) with a time-lapse interval of 0.1-1 seconds. To generate the evanescent wave, the laser was put at an angle of 65°, and the calculated evanescent wave field depth was 100 nm. Under these conditions, 1 pixel correlated to 153 nm. Transfected RBL-2H3 were kept in 750 μL of DMEM with 1% FCS in a climate-controlled chamber with 5% CO_2 at 37°C. Cells were activated by adding 250 μL of medium containing PMA and ionomycin as described under "Degranulation assays."

Quantitative image analysis

Image analysis was performed with the Volocity software suite (Version 5.2; Improvision). For colocalization of munc13-4–positive structures with

endosomal markers, we obtained z-stacks of at least 10 slices with optimal thickness for the pinhole. Slices of 0.15 μm were imaged on the Delta vision. We defined structures with Volocity in each channel by percentage of intensity, and separated the structures by size (< 0.5 μm). Thresholds for intensity were manually set on control samples, and 3D volumes were obtained. For analysis of size distribution, the average of 3D volumes was used. Positioning and relative position to the nucleus were evaluated manually on a single slice. To find overlap between structures identified in 2 independent channels, the 3D volumes were analyzed for overlap. For colocalization statistics, the total overlapping volume was compared with the total amount of volume per channel. Two-dimensional tracking of vesicles was done using the particle-tracking plug-in of ImageJ[25] using 0.3 μm for detection, displacement 4, link range 2. This yielded the highest number of tracks without nonsense jumps or fragmentation. On average, 60 tracks were analyzed per cell for 15 cells in 3 experiments; tracks shorter than 10 frames were discarded. Track coordinates were analyzed using Excel. The mean square displacement (MSD) was determined by plotting the distance between the first and last coordinate and plotting against Δ time. Granules were defined as immobile if the displacement at the last track was not larger than the detection limit of the granule (0.3 μm).

Statistical analysis

Statistical analysis of data was performed on the average of 3 independent experiments. To evaluate the statistical significance, we used single-factor ANOVA and *t* tests for individual significance between 2 samples. $P < .05$ was considered statistically significant.

Results

munc13-4 contains a novel rab27-binding motif

The molecular principles underlying directed membrane trafficking during degranulation of immune cells are not clear.[16,17,19,20] munc13-4 is an unusual rab27 effector in this pathway because it lacks a conserved rab27-binding domain (R27BD), does not need rab27 interaction for membrane association, and is the only known essential rab27 effector in cytotoxic lymphocytes. Rab27 binding requires aa 240-543,[10,21] but more precise information is not available. Interaction assays with additional truncations in GST pull downs showed that aa 240-543 is sufficient for rab27 binding (Figure 1A-B). N-terminal shortening of this munc13-4 fragment to aa 290-543 removed most of the binding capacity, suggesting that a major rab27-binding region is within aa 240-290 (Figure 1B), which contains the last residues of the first C2 domain, also known as the C2A domain. Complementary coimmunoprecipitation experiments of FLAG-rab27 with GFP-munc13-4 (aa 240-290) confirmed that this short construct retained the ability to bind rab27 in vivo (Figure 1C). We constructed a model for the 3D structure of munc13-4 C2A on the basis of the equivalent munc13-1 C2B domain structure[26] (Figure 1E). aa 240-290 encompass the C-terminal part (aa 240-284) of the C2A domain (aa 109-284), including its 3 last β-strands (designated here βA, βB, and βC). This region is conserved among munc13 proteins, but the rab27-binding determinant is specific for munc13-4 (supplemental Figure 1A, available on the *Blood* Web site; see the Supplemental Materials link at the top of the online article). In agreement with this, we found little if any binding to other munc13 family members (supplemental Figure 1B). We then performed alanine scan mutagenesis on aa 240-291 in full-length munc13-4 by replacing sequential groups of 3 amino acids with alanine residues. Interaction assays with the point mutants showed that munc13-4(FQL > AAA) and munc13-4(IHK > AAA) mutants lost 80% of their rab27a binding, whereas a gapped construct munc13-4Δ (aa 280-285) lacking the FQLIHK residues confirmed their requirement (Figure 1F). The sequence of this region is only modestly conserved among munc13 family members (supplemental Figure 1A). Flanking amino acids contributed to the interaction surface, because mutations in these gave an intermediate binding phenotype (Figure 1D). YFP-munc13-4(FQL > AAA) and YFP-munc13-4Δ (280-285) localized correctly with $CD63^+$ lysosomes in RBL-2H3 cells (supplemental Figure 2 left column), and quantitation of secretory lysosome diameter, localization, and distance to the nucleus all showed that these were not significantly affected (not shown). A small fraction (< 10%) of wild-type munc13-4 and mutants localized to early endosomes containing EEA1 (supplemental Figure 2 right column). Because misfolded munc13-4 is distributed entirely to the cytoplasm,[21] and the 2 mutants are associated with CD63 structures (supplemental Figure 2 right column), impaired rab27a binding is not an indirect effect caused by misfolding. Limited proteolysis experiments of the mutants with endoproteinase Glu-C and proteinase K gave the same digestion patterns as wild-type protein by SDS-PAGE (not shown), whereas the munc13-4Δ (aa 608-611) FHL3 mutant does not.[21] These results show that rab27a binding is not required for localization of munc13-4 to secretory lysosomes or for secretory lysosome positioning.

munc13-4–rab27 interaction is required for CTL degranulation

We next analyzed the functionality of the munc13-4–rab27a complex in secretory lysosome (cytotoxic granule) exocytosis. CFP-tagged munc13-4 constructs were expressed in munc13-4–deficient CTLs from an FHL3 patient, who represents a natural human munc13-4–knockout model. Degranulation was then evaluated by the appearance of the granule-associated CD107 on the surface of CTLs after cell stimulation with an antibody against the TCR CD3 subunit. Like the FHL3 munc13-4Δ (aa 608-611) mutant, and in contrast to wild-type munc13-4, point mutations in R27BD and munc13-4Δ (aa 280-285) were unable to rescue degranulation (Figure 2A-B). Mutant construct munc13-4(PDR > AAA), which preserved rab27a binding, restored degranulation to similar levels as wild-type munc13-4, whereas munc13-4(RRA > AAA), with intermediate binding, gave a partial rescue (Figure 2A-B). Therefore, the molecular interaction between munc13-4 and rab27a regulates a critical step of the cytotoxic granule pathway in lymphocytes.

munc13-4 interaction with rab27 is essential for degranulation in RBL-2H3 cells

We next investigated whether this role of munc13-4 and rab27a was specific for CTLs or if it might also occur in immune cells that degranulate in a nonpolarized manner[21,27,28] via compound exocytosis. This exocytosis modality allows for the instantaneous release of secretory lysosome content[29] on immune receptor signaling. We used a robust complementation assay in RBL-2H3 cells[23] in which siRNA-resistant YFP-munc13-4 constructs are expressed from lentiviruses, and endogenous rat munc13-4 is knocked down to < 15% by 2 siRNAs (Figure 2C). FcεR was cross-linked with IgE and TNP-BSA, and stimulated release of β-hexosaminidase was used as readout for secretory lysosome degranulation. In agreement with degranulation experiments in FHL3-cytotoxic lymphocytes, munc13-4 mutants that poorly bind rab27a, also yielded minimal recovery in mast cell degranulation (Figure 2D).

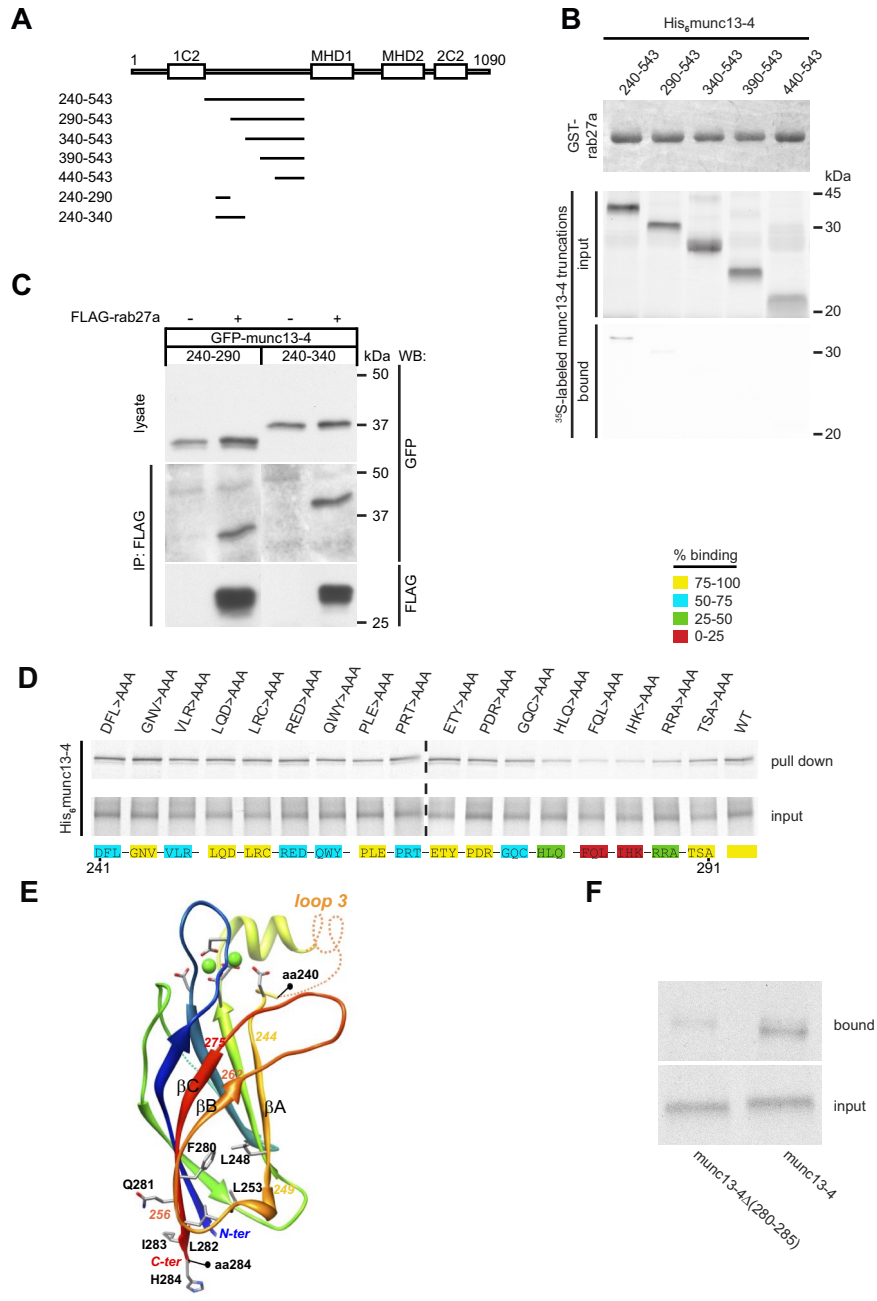

Figure 1. Critical residues in munc13-4 required for rab27 binding. (A) Organization of munc13-4 and truncations used in this study. (B) Binding assay of ^{35}S-labeled His$_6$munc13-4 truncations and GSTrab27aGTPγS. Bound proteins were resolved on a 10% SDS-PAA gel and visualized by phosphor imaging. (C) FLAG-tagged rab27a and GFP-munc13-4 truncations were coexpressed in COS-7 cells. Anti-FLAG immunoprecipitates were analyzed by Western blot with a GFP mAb. (D) Binding assay of ^{35}S-labeled His$_6$munc13-4 AAA mutants and GSTrab27aGTPγS. Bound protein was eluted and assayed by phosphor imaging. The amino acid sequence containing the R27BD is given at the bottom of the panel, and the coloring of the blocks indicates the percentage binding as per the legend in the panel. (E) Model of the 3D structure of the C2A domain of munc13-4 (aa 111-284, ribbon diagram). The model was made on the basis of the alignment[8] of the C2A domain of human munc13-4 with the C2B domain of rat munc13-1, for which the experimental 3D structure (pdb 3kwu) has been solved.[26] The limits of the 240-284 segment, which includes the β-strands βA to βC, are shown, as well as the amino acids discussed in the text. Loops that were not modeled are symbolized with dashed lines. Amino acids of the Ca^{2+}-binding site are shown, together with the bound Ca^{2+} ions (green spheres). (F) Binding assay of ^{35}S-labeled His$_6$munc13-4Δ (280-285) or His$_6$munc13-4 and GSTrab27aGTPγS. Bound protein was eluted and assayed by phosphor imaging. Quantitations of signals present in bound and total samples and background correction were done with the ImageQuant software package.

Degranulation was less efficiently inhibited in mast cells than in FHL3 CTLs, which probably reflects the small residual level of nonsilenced munc13-4. We conclude that the munc13-4–rab27 complex is essential in secretory lysosome release in immune cells.

munc13-4 regulates merger of rab11 and rab27a endosomes independently of rab27a

munc13-4 serves a role in maturation of secretory lysosomes, where it is needed for merger of rab27a-containing late endosomes and rab11-positive recycling endosomes[10] into a precursor exocytic endosome. Using the munc13-4 R27BD point mutants, we investigated whether this function of munc13-4 involves rab27a. In FHL3 CTLs cotransfected with DsRed-rab11, GFP-rab27a, and CFP-munc13-4 constructs, we analyzed the codistribution of rab11- and rab27-labeled structures (Figure 3A). Ectopically expressed munc13-4 or munc13-4 R27BD point mutants similarly increased the number of merged rab11$^+$ and rab27a$^+$ structures compared with control CTLs or those from an FHL3 patient. We then investigated whether the requirement for munc13-4 in maturation of secretory lysosomes could be extended to other immune cells. Introduction of YFP-munc13-4 in RBL-2H3 cells expressing CFP-rab11 and Cherry-rab27a gave a significant increase in colocalization between rab11 and rab27a compared with cells that were not transfected with YFP-munc13-4 (supplemental Figure 3A-B), irrespective of their activation state. Knockdown of endogenous munc13-4 did not significantly affect the extent of colocalization between CFP-rab11 and Cherry-rab27a compared with nonsilenced control cells (supplemental Figure 3). It is possible that residual endogenous munc13-4 (Figure 2) was sufficient to sustain

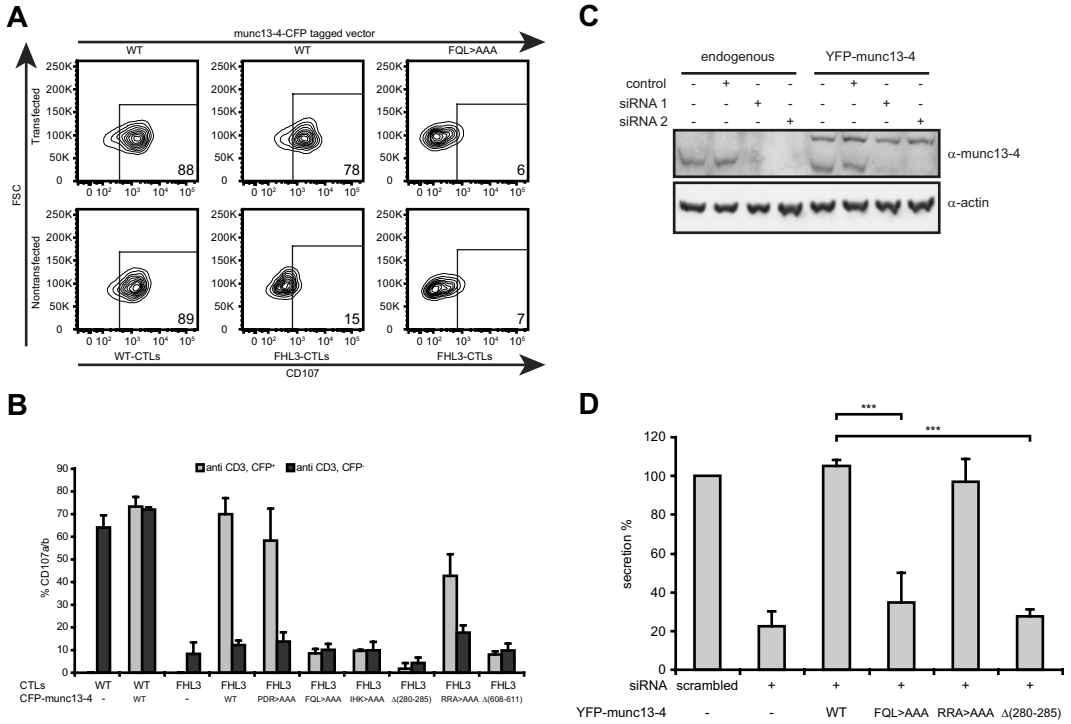

Figure 2. The munc13-4–rab27a interaction is required for degranulation. (A) CTLs from a control (WT-CTLs) or munc13-4–deficient patient (FHL3-CTLs) were transfected with CFP-munc13-4 wild-type (WT) or CFP-munc13-4 (FQL > AAA) mutant construct. In each experiment, the CFP^+ (transfected) and CFP^- (nontransfected) cell populations were tested for CD107 expression after stimulation with anti-CD3. Numbers indicate the percentage of degranulating CTLs. The data shown are representative of 3 independent experiments with similar results. (B) CTLs from a control (WT) or munc13-4–deficient patient (FHL3) were transfected with various CFP-munc13-4 constructs (WT or mutants) as indicated and the transfected (gray) and untransfected (black) cell populations were analyzed as in panel A. Values represent means (± SD) percentages of the $CD107^+$ CTLs. The results shown are representative of 3 independent experiments with similar results. (C) RBL-2H3 cells with and without ectopically expressed YFP-munc13-4 were transfected with 2 siRNAs targeting different regions in rat munc13-4 by AMAXA nucleofection. Cell lysates were analyzed by Western blot with a polyclonal antibody against munc13-4 and a mAb against actin. (D) RBL-2H3 cells stably expressing indicated wild-type and mutant YFP-munc13-4 constructs were transfected with siRNA #2 or control siRNA as in panel A. Cells were activated as described in "Methods," and β-hexosaminidase activity was determined colorimetrically. Percentage secreted is calculated as fraction of total amount of β-hexosaminidase activity present in a parallel dish of the same cell line that was not stimulated. We then set the extent of secretion in the cells treated with scrambled siRNA to 100%, and normalized the other results to this value. ***$P < .005$.

coalescence of rab11 and rab27a membranes (supplemental Figure 3B). When we combined silencing of endogenous munc13-4 with expression of YFP-munc13-4Δ (aa 280-285), we obtained nearly identical colocalization for rab11 and rab27a as with wild-type YFP-munc13-4 in resting (Figure 3B-C) and activated (not shown) cells. The localization experiments confirmed a function for munc13-4 in maturation of secretory lysosomes. These observations extend previous studies in CTLs from GS2 patients, in whom munc13-4 increased coupling of rab11 and late-endocytic organelles in the absence of rab27a.[10]

Impaired rab27 binding reduces tethering of munc13-4 vesicles

To understand how rab27 and munc13-4 coordinately control secretory lysosome release, we analyzed their dynamic behavior in RBL-2H3 cells expressing Cherry-rab27a and YFP-munc13-4 using TIRF microscopy. We observed 2 populations of YFP-munc13-4–Cherry-rab27a–containing granules (Figure 4A): a group of small, 0.3-μm subplasmalemmal structures that was distinct in diameter from the stationary large (> 2 μm) multigranular clusters observed by epifluorescence microscopy in the perinuclear cytoplasm (supplemental Figure 2 left column). The smaller peripheral granules were mobile and moved from the interior of the cell to the TIRF zone and back. The large clusters seldom appeared in the TIRF zone (Figure 4B) and were less fluorescent than the small granules (Figure 4A).

Cherry-rab27a YFP-munc13-4 cells were then silenced for endogenous munc13-4 and the mobility of Cherry-rab27a YFP-munc13-4 granules quantified by assaying their trajectories using TIRF microscopy. The MSD of the trajectories was plotted against time interval (Δt) averaged over all tracks. We also scored the fraction of mobile granules, defined as granules with MSDs larger than their own diameter of 0.3 μm. In Cherry-rab27a YFP-munc13-4 cells, many (~ 50%) of the granules were immobile at the plasma membrane, whereas others made diffuse tracks along the cell surface. After activation by ionomycin and PMA, the granules became less mobile (supplemental Videos 1-2), which resulted in diminished displacement (Figure 4A,C). The fraction of mobile granules was significantly decreased in the activated cells, suggesting increased entrapment and corralling of the granules at the plasma membrane (Figure 4C,E) in parallel with the stimulated release of β-hexosaminidase (Figure 2D). MSD versus time interval (Δt) plots show negative curvature and will therefore eventually approach an asymptote, reflecting space-constrained movement. The radius of the constrained space is defined by the square root of the asymptote value. For Cherry-rab27a YFP-munc13-4 granules, the radius was reduced from 0.57 μm to 0.41 μm upon activation. Impaired mobility in this analysis (Figure 4C,E) reflects enhanced tethering of the granules to the plasma membrane, as was originally shown for dense core granules in neuroendocrine cells.[30-32]

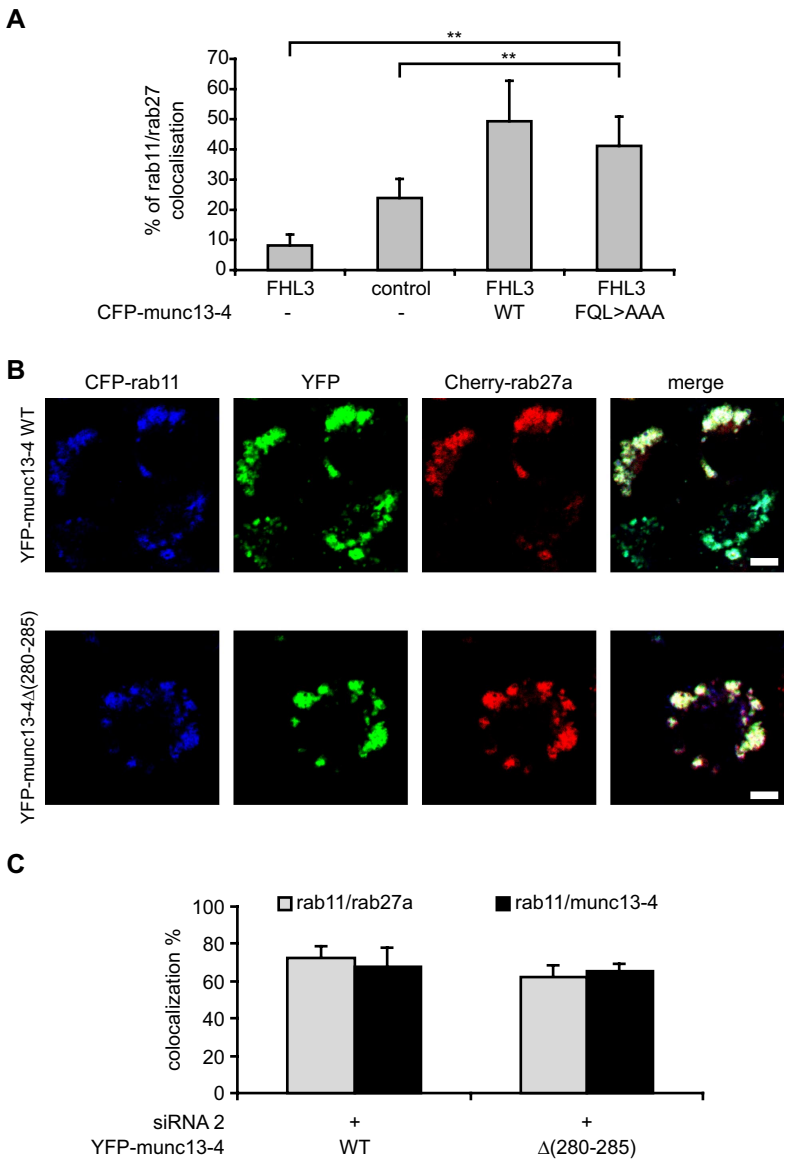

Figure 3. Endosome coalescence occurs independently of the munc13-4 rab27 complex. (A) Quantitative analysis of rab11-rab27a–overlapping structures in control or munc13-4–deficient (FHL3) CTLs coexpressing DsRed-rab11 and GFP-rab27a as described previously.[10] FHL3 CTLs were also cotransfected with wild-type (WT) or the munc13-4(FQL > AAA) construct. Data represent statistical image analysis of 2-color pixel intensity correlation in all optical sections and are the average (± SD) of the overlapping surface calculated by computer-assisted image analysis of at least 10 cells. (B) Confocal microscopy of RBL-2H3 cells stably expressing CFP-rab11 (blue), Cherry-rab27a (red), and YFP-munc13-4 constructs (green); endogenous rat munc 13-4 was silenced with siRNA #2. (C) Quantitation of codistribution of rab11 with munc13-4 and rab27a. Colocalization was determined in 10 cells using Volocity as described in the "Methods," and is displayed as a percentage of rab11 over munc13-4 (black) and rab11 over rab27a (gray). Error bars are SEM of 3 experiments. Scale bars indicate 5 μm. $^{**}P < .01$.

In cells expressing YFP-munc13-4(FQL > AAA) and YFP-munc13-4Δ (aa 280-285) mutants, the typical activation-induced mobility changes were not observed (Figure 4D-E). This suggested that the rab27-binding mutants have reduced tethering/docking capabilities and that the interaction of munc13-4 with rab27a is needed to allow granules to effectively dock and fuse at the plasma membrane. Although Cherry and YFP fluorophores could not be simultaneously imaged using our microscopy system, we consistently obtained identical data for Cherry-rab27a and YFP-tagged constructs in the double-transduced cell line. To rule out that the activity-dependent change in mobility was caused by overexpression of YFP-munc13-4, we used Cherry-rab27a single transfectants and obtained the same results (data not shown). The TIRF microscopy experiments showed that the mutants have reduced tethering-docking capabilities and that the interaction of munc13-4 with rab27a is needed to allow granules to effectively dock at the plasma membrane.

Discussion

CTLs harbor distinct secretory compartments for storage of cytokines and lytic molecules, the release of which occurs via different signaling and trafficking pathways. The orchestration of these events presumably requires sophisticated levels of control.[33] In the present study, we describe a general mechanism for the regulation of secretory lysosome release by a complex of the small GTPase rab27 and munc13-4. First, we defined a new rab27a-binding motif on munc13-4, which allowed the dissection of rab27-dependent and -independent functions. Second, we showed that point mutants with impaired rab27a binding failed to complement loss of degranulation, because tethering secretory lysosomes to the plasma membrane is inhibited. Third, we found that the rab27-independent function of munc13-4 is a general property of hematopoietic cells for secretory lysosome maturation.

The 3D structures of rab27b with melanophilin[34] and rab27a with slp-2a[35] define a conserved R27BD formed by 2 linked α-helical regions. munc13-4 aa 240-290 does not resemble this binding site. It includes the last 3 β-strands of the C2A domain (aa 240-284; Figure 1E) and a basic sequence (aa 285-290), which links the C2A domain to the following MUN domain. The critical aa 280-285 are at the edge of C2A and therefore outside the context of the full-length C2A domain. The structure of the 240-284

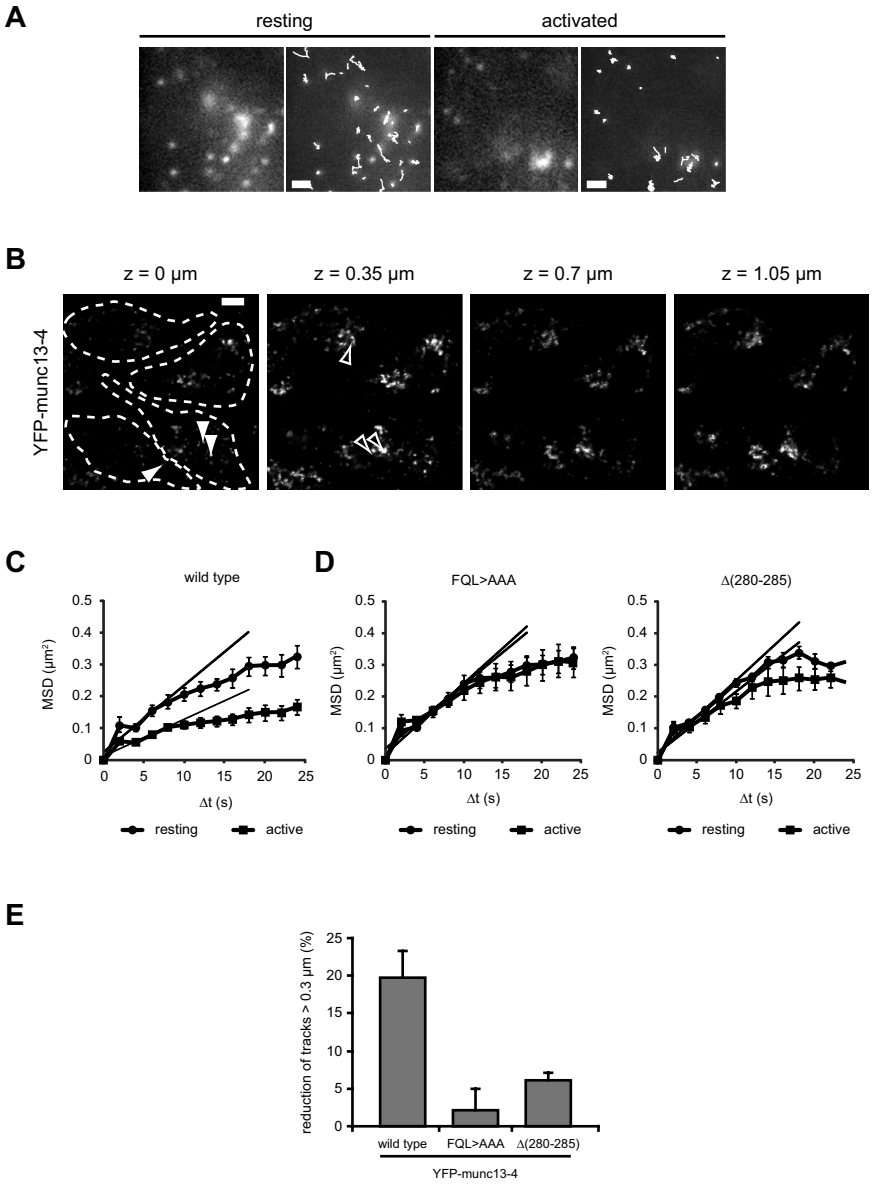

Figure 4. Docking of munc13-4 granules at the plasma membrane requires rab27. (A) TIRFM view of YFP-munc13-4 in resting and activated RBL-2H3 stably expressing Cherry-rab27a and YFP-munc13-4. White trajectories represent tracks of individual granules. Scale bar indicates 2 μm. (B) RBL-2H3 cells expressing YFP-munc13-4 were imaged with a confocal microscope using 0.35-μm slices. The smaller granules (closed arrowheads) that are observed in the TIRF view are predominantly found at the basal side of the cell (z = 0 μm), whereas the signal for the out-of-focus, larger granules in the background is indicated with open arrowheads. Note that the optical sections are ~ 3 times thicker than the TIRF zone. The larger granules with diameter > 0.3 μm are distributed to the upper layers of the z-stack. Scale bar indicates 5 μm. (C) MSD versus Δtime plots of the tracks analyzed per cell (n = 15) in resting (●) or activated (■) Cherry-rab27a YFP-munc13-4–expressing cells of a representative experiment. Black lines indicate the slope of the first 8 seconds. (D) Same analysis as in panel C for Cherry-rab27a YFP-munc13-4(FQL > AAA) and Cherry-rab27a YFP-munc13-4Δ (280-285) cell lines. (E) Decrease in mobile vesicles after activation was analyzed per cell for 15 cells in 3 experiments and compared between wild-type munc13-4 and mutants that do not bind rab27.

segment as present in the full-length globular and well-folded C2A domain may be lost in the truncations studied here. Conversely, because in the complete C2A domain, strand βB forms a β-hairpin with the βC-strand, which includes the critical 280-285 residues, it is attractive to theorize that such a local structure is maintained in the truncated proteins. Moreover, the partners of the amino acid residues that in strand βC participate in the hydrophobic core of the C2A domain (F280 and L282) are found in strand βA (L248) and in the loop linking βA and βB (L253). Therefore, it is a distinct possibility that a local "C2A-like" structure is maintained in the truncated proteins, which permits binding of rab27a at the level of the bottom of the C2A domain and of its C-terminal extension (Figure 2B). This hypothesis is supported by the fact that a similar region of the C2 domain (the bottom tip and its C-terminal extension) is involved in the munc13-1 C2A domain heterodimerization with the RIM Zn-finger.[36] Accordingly, the substitutions of aa 285-290 in alanine residues should either disrupt the fold (F280 and L282) or interfere directly in the binding event (Q281, I283, H284, and K285). The correct localization of the munc13-4 constructs suggests that the second hypothesis is more likely.

Elucidation of the rab27a-binding region was essential for understanding the role of the multidomain protein munc13-4 in secretory lysosome functions, particularly because the significance of the interaction with rab27 has been enigmatic. In resting mast cells, they colocalize extensively on the limiting membrane of secretory lysosomes,[21] suggesting constitutive residence of the complex at this location. In NK cells, however, an external signal is required for colocalization of rab27 and munc13-4.[19] In CTLs, munc13-4 codistributes with the recycling endosome marker rab11 and is important for their merging with rab27$^+$ late endocytic organelles. Our functional localization experiments of rab11 and rab27 in CTLs and RBL-2H3 showed that munc13-4, irrespective of rab27 binding, directs the merger of exocytic rab11$^+$ and late endosomal rab27$^+$ compartments. It is also in agreement with the absence of a maturation phenotype in CTLs of GS2 patients.[10] It will be interesting to understand how munc13-4 can bring together rab11 and rab27 membranes. Possible mechanisms include scenarios in which munc13-4 in complex with an accessory protein binds directly to rab11. Alternatively, it could sample the rab11 effector network to bridge rab27 and rab11 membranes. The

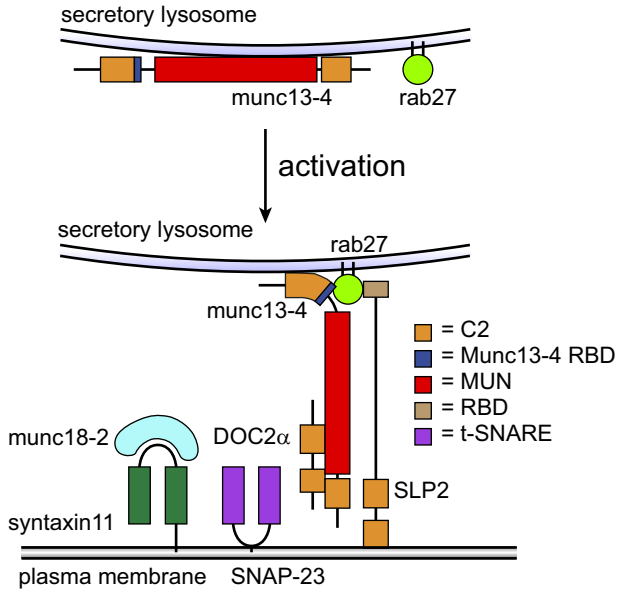

Figure 5. Hypothetical model for function of munc13-4 and rab27. Activation of cells targets munc13-4 and rab27 to each other's vicinity, establishing a specific domain on secretory lysosomes. Colocalization facilitates the interaction between the 2 proteins and, because rab27 and munc13-4 have independent membrane-binding determinants, their interaction enhances the affinity of the complex for the secretory lysosome membrane. At this point, the interaction with rab27 could fold munc13-4 in a conformation that allows the first C2 domain to bridge the apposing bilayers of secretory lysosome and plasma membrane.[50] The complex can now serve as nucleation point or coincidence detection unit for interaction with other proteins important for secretory lysosome release. The C-terminal part of munc13-4 might bind to syntaxin-11 or engage Doc2α, which then interacts with SNAP-23, establishing a regulatory circuit for controlling a cognate SNARE complex for fusion with the plasma membrane. The interaction with rab27-GTP secures the recruitment of slp2 and other effectors involved in tethering the secretory lysosome to the plasma membrane. Loss of rab27 binding uncouples these events and interferes with degranulation.

formation of secretory lysosomes, and the connections between them and with other granules, have only recently become subject of investigation. The propensity to use munc13-4 for bringing together rab11 and rab27 compartments suggests a fundamental role of rab11-containing recycling endosomes in supplying exocytic machinery[37,38] to immature secretory lysosomes in immune cells. KIF13A and the adaptor AP-1 are 2 other regulators of traffic through recycling endosomes that have been implicated in the function of melanosomes, a secretory lysosome–related organelle.[39] This complex establishes a recycling endosomal domain that partially overlaps with rab11[39] and may cooperate in cargo sorting because it positions endosomes close to secretory lysosomes in the cell periphery, facilitating interorganellar connections. The aggregate data provide strong arguments for a role of recycling endosomes with rab11 in the maturation of secretory lysosomes. Although this is an appealing general mechanism, cell-type-specific regulation needs to be imposed, because melanocytes, for example, do not express munc13-4.[21] However, this might merely reflect the deployment of alternative rab11 effector networks in different cell types for related purposes.

What could be the molecular mechanism for the activity of the rab27 munc13-4 complex? Other munc13s share the canonical organization of tandem C2 domains separated by the MUN domain.[26] In contrast to munc13-4, however, they do not bind rab27. Instead, the N-terminal extension of munc13-1 serves as an interaction node with rab3 and matrix proteins, which regulates the activity of presynaptic neurons.[40] In munc13-4, this property might be conferred by interactions at the interface of the C2A and MUN domains with rab27. The MUN domain of munc13-1 can bind syntaxin-1 and SNAP25 in liposomes, and competes with munc18-1[41] to promote SNARE complex assembly. The homologous region in munc13-4 could similarly regulate syntaxin-11[42] and SNAP 23,[43] which are thought to be involved in the late stages of lysosome secretion. The v-SNARE VAMP8 is also required for exocytosis of lytic granules[44] and binds SNAP23,[45] suggesting a functional relationship among syntaxin-11, SNAP23, and VAMP8 in secretory lysosome fusion with the plasma membrane. The interaction with rab27a-GTP and Doc2α[46] within the MUN domain conceivably controls the activity of the MUN domain in removing munc18-2 and opening syntaxin-11 (Figure 5). Because docking and priming steps in membrane fusion are dependent processes,[47] it is likely that the role of rab27a and munc13-4 might extend beyond priming. The MUN domain shares homology with helical rod components of the CATCHR family of tethering complexes, including sec6 of the exocyst and vps53 of GARP.[48,49] It is possible that the complex of rab27 and munc13-4 forms a coincidence detection unit for recruitment of tethering factors such as slp family members to facilitate the capture and retention of secretory lysosomes at the plasma membrane (Figure 5), enhancing the probability for the assembly of cognate SNARE complexes.

Acknowledgments

The authors thank Rene Scriwanek for help with preparation of the figures.

The study was funded by the Dutch Cancer Society Koningin Wilhelmina Fonds (to P.v.d.S.), Inserm, the French National Research Agency (ANR), and the Fondation pour la Recherche Médicale (FRM). N.N. is supported by a postdoctoral fellowship from l'Association de Recherche contre le cancer (ARC). Core facilities in Paris were partly financed by the Imagine Foundation and in Utrecht by the Netherlands Organization for Medical Research (ZonMW).

Authorship

Contribution: E.D.E., M.N., N.T.N., J.V., P.M.P.v.B.H., G.d.S.B., and P.v.d.S. conceived of and designed the experiments; M.C., E.D.E., M.G., M.N., N.T.N., P.v.d.S., and J.V. performed the experiments; E.D.E., H.C.G., M.N., N.T.N., J.V., I.C., P.M.P.v.B.H., G.d.S.B., and P.v.d.S. analyzed the data; and G.d.S.B. and P.v.d.S. wrote the manuscript.

Conflict-of-interest disclosure: The authors declare no competing financial interests.

Correspondence: Peter van der Sluijs, Department of Cell Biology, UMC Utrecht, 3584 CX Utrecht, The Netherlands; e-mail: p.vandersluijs@umcutrecht.nl.

References

1. Voskoboinik I, Smyth MJ, Trapani JA. Perforin mediated target cell death and immune homeostasis. *Nat Rev Immunol.* 2006;6(12):940-951.
2. Stinchcombe J, Bossi G, Griffiths GM. Linking albinism and immunity: The secrets of the secretory lysosome. *Science.* 2004;305(5680):55-59.
3. Pachlopnik Schmid J, Côte M, Ménager MM, et al. Inherited defects in lymphocyte cytotoxic activity. *Immunol Rev.* 2010;235(1):10-23.
4. Stinchcombe J, Majorovits E, Bossi G, Fuller S, Griffiths GM. Centrosome polarization delivers

secretory granules to the immunological synapse. *Nature.* 2006;443(7110):462-465.

5. Griffiths GM, Tsun A, Stinchcome JC. The immunological synapse: a focal point for endocytosis and exocytosis. *J Cell Biol.* 2010;189(3):399-406.
6. Stinchcombe JC, Bossi G, Booth S, Griffiths G. The immunological synapse of CTL contains a secretory domain and membrane bridges. *Immunity.* 2001;15(5):751-761.
7. Ménasché G, Pastural E, Feldmann J, et al. Mutations in rab27a cause Griscelli's syndrome associated with haemophagocytic syndrome. *Nat Genet.* 2000;25(2):173-176.
8. Feldmann J, Callebaut I, Raposo G, et al. Munc13-4 is essential for cytolytic granules fusion and is mutated in a form of familial hemophagocytic lymphohistiocytosis (FHL3). *Cell.* 2003; 115(4):461-473.
9. Marcenaro S, Gallo F, Martini S, et al. Analysis of NK cell function in FHL; defective CD107a surface expression heralds munc13-4 defect and discriminates between genetic subtypes of the disease. *Blood.* 2006;108(7):2316-2323.
10. Ménager MM, Menasche G, Romao M, et al. Secretory cytotoxic granule maturation and exocytosis require the effector protein hMunc13-4. *Nat Immunol.* 2007;8(3):257-267.
11. Stenmark H. Rab GTPases as coordinators of vesicle traffic. *Nat Rev Mol Cell Biol.* 2009;10(8): 513-525.
12. Fukuda M. Versatile role of rab27 in membrane trafficking: focus on the rab27 effector families. *J Biochem.* 2005;137(1):9-16.
13. Itzen A, Goody RS. Key determinants of rab specificity. *Structure.* 2008;16(10):1437-1439.
14. Holt O, Kanno E, Bossi G, et al. Slp1 and slp2-a localize to the plasma membrane of CTL and contribute to secretion at the immunological synapse. *Traffic.* 2008;9(4):446-457.
15. Ménasché G, Menager MM, Lefebre JM, et al. A newly identified isoform of slp2-a associates with rab27a in cytotoxic T cells and participates to cytotoxic T cell deganulation. *Blood.* 2008;112(13): 5052-5062.
16. Tolmachova T, Abrink M, Futter CE, Authi KS, Seabra MC. Rab27b regulates number and secretion of platelet dense granules. *Proc Natl Acad Sci U S A.* 2007;104(14):5872-5877.
17. Ren Q, Wimmer C, Chicka MC, et al. Munc13-4 is a limiting factor in the pathway required for platelet granule release and hemostasis. *Blood.* 2010; 116(6):869-877.
18. Johnson JL, Hong H, Monfregola J, Kiosses WB, Catz SD. Munc13-4 restricts motility of rab27a expressing vesicles to facilitate lipopolysaccharide-induced priming of exocytosis in neutrophils. *J Biol Chem.* 2011;286(7):5647-5656.
19. Wood SM, Meeths M, Chiang SCC, et al. Different NK cell activating receptors preferentially recruit rab27a or munc13-4 to perforin containing granules for cytotoxicity. *Blood.* 2009;114(19): 4117-4127.
20. Bryceson YT, Ljunggren HG, Long EO. Minimal requirement for induction of natural cytotoxicity and intersection of activation signals by inhibitory receptors. *Blood.* 2009;114(13):2657-2666.
21. Neeft M, Wieffer M, de Jong AS, et al. Munc13-4 is and effector of rab27a and controls secretion of lysosomes in haematopoietic cells. *Mol Biol Cell.* 2005;16(2):731-741.
22. Hoogenraad CC, Popa I, Futai K, et al. Neuron specific rab4 effector GRASP-1 coordinates membrane specialization and maturation of recycling endosomes. *PLoS Biol.* 2010;8(1): e1000283.
23. Elstak E, de Jong A, van der Sluijs P. A platform for complementation and characterization of familial haemophagocytic lymphohistiocytosis 3 mutations. *J Immunol Methods.* 2011;358(1-2): 58-66.
24. Betts MR, Brenchley JM, Price DA, et al. Sensitive and viable identification of antigen-specific CD8+ T cells by a flow cytometric assay for degranulation. *J Immunol Methods.* 2003;281(1-2): 65-78.
25. Sbalzarini IF, Koumoutsakis P. Feature point tracking and trajectory analysis for video imaging in cell biology. *J Struct Biol.* 2005;151(2):182-195.
26. Shin OH, Lu J, Rhee JS, et al. Munc13 C2B domain is an activity-dependent Ca2+ regulator of synaptic exocytosis. *Nat Struct Mol Biol.* 2010; 17(3):280-288.
27. Brzezinska AA, Johnson JL, Munafo DB, et al. The rab27a effectors jfc1/slp1 and munc13-4 regulate exocytosis of neutrophil granules. *Traffic.* 2008;9(12):2151-2164.
28. Pivot-Pajot C, Varoqueaux F, de Saint Basile G, Bourgoin SG. Munc13-4 regulates secretion in human neutrophils. *J Immunol.* 2008;180(10): 6786-6797.
29. Pickett JA, Edwardson JM. Compound exocytosis: mechanisms and functional significance. *Traffic.* 2006;7(2):109-116.
30. Nofal S, Becherer U, Hof D, Matti U, Rettig J. Primed vesicles can be distinguished from docked vesicles by analyzing their mobility. *J Neurosci.* 2007;27(6):1386-1395.
31. Oheim M, Stuhmer W. Trafficking chromaffin granules on their way through the actin cortex. *Eur Biophys J.* 2000;29(2):67-89.
32. Xia S, Xu L, Bai L, Xu ZQ, Xu T. Labeling and dynamic imaging of synaptic vesicle-like microvesicles in PC12 cells using TIRFM. *Brain Res.* 2004;997(2): 159-164.
33. Huse M, Quann EJ, Davis MM. Shouts, whispers and the kiss of death: directional secretion in T cells. *Nat Immunol.* 2008;9(10):1105-1111.
34. Kukimoto-Niino M, Sakamoto A, Kanno E, et al. Structural basis for the exclusive specificity of slac2-a/melanophilin for the rab27 GTPases. *Structure.* 2008;16(10):1478-1490.
35. Chavas LMG, Ihara K, Kawasaki M, et al. Elucidation of rab27 recruitment by its effectors: structure of rab27a bound to exophilin4/slp2-a. *Structure.* 2008;16(10):1468-1477.
36. Lu JC, Machius M, Dulubova I, et al. Structural basis for a munc13-1 homodimer to munc13-1/RIM heterodimer switch. *PLoS Biol.* 2006;4(7): e192.
37. Khandelwal P, Ruiz WG, Balesteire-Hawryluk E, Weisz OA, Goldenring JR, Apodaca G. Rab11a-dependent exocytosis of discoidal/fusiform vesicles in bladder umbrella cells. *Proc Natl Acad Sci U S A.* 2008;105(41):15773-15778.
38. Sagi-Eisenberg R. The mast cell: where endocytosis and regulated exocytosis meet. *Immunol Rev.* 2007;217:292-303.
39. Delevoye C, Hurbain I, Tenza D, et al. AP-1 and KIF13A coordinate endosomal sorting and positioning during melanosome biogenesis. *J Cell Biol.* 2009;187(2):247-264.
40. Wang X, Hu B, Zieba A, et al. A protein interaction node at the neurotransmitter release site: domains of Aczonin/Piccolo, Bassoon, CAST, and rim converge on the N-terminal domain of Munc13-1. *J Neurosci.* 2009;29(40):12584-12596.
41. Weninger K, Bowen ME, Choi UB, Chu S, Brunger AT. Accessory proteins stabilize the acceptor complex for synaptobrevin, the 1:1 syntaxin/SNAP-25 complex. *Structure.* 2008;16(2): 308-320.
42. Bryceson YT, Rudd E, Zheng C, et al. Defective cytotoxic lymphocyte degranulation in syntaxin-11 deficient familial hemophagocytic lymphohistiocytosis 4 (FHL4) patients. *Blood.* 2007;110(6):1906-1915.
43. Valdez AC, Cabaniols JP, Brown MJ, Roche PA. Syntaxin 11 is associated with SNAP-23 on late endosomes and the trans-Golgi network. *J Cell Sci.* 1999;112(6):845-854.
44. Dressel R, Elsner L, Novota P, Kanwar N, Fischer von Mollard G. The exocytosis of lytic granules is impaired in Vtib or Vamp8 deficient CTL leading to a reduced cytotoxic activity following antigen specific activation. *J Immunol.* 2010; 185(2):1005-1014.
45. Paumet F, le Mao J, Martin S, et al. Soluble NSF attachement protein receptors (SNAREs) in RBL-2H3 mast cells: Functional role of syntaxin 4 in exocytosis and identification of a vesicle-associated membrane protein 8-containing secretory compartment. *J Immunol.* 2000;164(11):5850-5857.
46. Higashio H, Nishimura N, Ishizaki H, et al. Doc2a and munc13-4 regulate Ca2+ dependent secretory lysosome exocytosis in mast cells. *J Immunol.* 2008;180(7):4774-4784.
47. Yizhar O, Ashery U. Modulating vesicle priming reveals that vesicle immobilization is necessary but not sufficient for fusion competence. *PLoS One.* 2008;3(7):e2694.
48. Pei J, Ma C, Rizo J, Grishin NV. Remote homology between munc13 MUN domain and vesicle tethering complexes. *J Mol Biol.* 2009;391(3): 509-517.
49. Hughson F, Reinisch K. Structure and mechanism in membrane trafficking. *Curr Opin Cell Biol.* 2010;22(4):454-460.
50. Araç D, Chen X, Khant HA, et al. Close membrane-membrane proximity induced by Ca^{2+}-dependent multivalent binding of synaptotagmin-1 to phospholipids. *Nat Struct Mol Biol.* 2006; 13(3):209-217.